Entangled singularity patterns of photons in Ince-Gauss modes

Mario Krenn,[1,2,*] Robert Fickler,[1,2] Marcus Huber,[3] Radek Lapkiewicz,[1,2] William Plick,[1,2]
Sven Ramelow,[1,2] and Anton Zeilinger[1,2,4,*]

[1]*Quantum Optics, Quantum Nanophysics, Quantum Information, University of Vienna, Boltzmanngasse 5, Vienna A-1090, Austria*
[2]*Institute for Quantum Optics and Quantum Information, Boltzmanngasse 3, Vienna A-1090, Austria*
[3]*University of Bristol, Department of Mathematics, Bristol BS8 1TW, United Kingdom*
[4]*Vienna Center for Quantum Science and Technology, Faculty of Physics, University of Vienna, Boltzmanngasse 5, Vienna A-1090, Austria*

(Received 21 November 2012; published 23 January 2013)

Photons with complex spatial mode structures open up possibilities for new fundamental high-dimensional quantum experiments and for novel quantum information tasks. Here we show entanglement of photons with complex vortex and singularity patterns called Ince-Gauss modes. In these modes, the position and number of singularities vary depending on the mode parameters. We verify two-dimensional and three-dimensional entanglement of Ince-Gauss modes. By measuring one photon and thereby defining its singularity pattern, we nonlocally steer the singularity structure of its entangled partner, while the initial singularity structure of the photons is undefined. In addition we measure an Ince-Gauss specific quantum-correlation function with possible use in future quantum communication protocols.

DOI: 10.1103/PhysRevA.87.012326 PACS number(s): 03.67.Bg, 03.67.Hk, 42.50.Tx, 42.65.Lm

I. INTRODUCTION

Quantum entanglement is one of the most significant features of quantum mechanics. It is used in quantum information protocols for quantum cryptography, quantum teleportation, and quantum computation [1]. Qubit entanglement of photons has been shown in various degrees of freedom, such as polarization [2], time and energy [3], path [4], or frequency [5]. In addition, photons can also be entangled in orbital angular momentum (OAM) states [6]. These so-called Laguerre-Gauss (LG) modes define a discrete, infinite-dimensional Hilbert space [7,8] and have been used in fundamental experiments concerning higher-dimensional entanglement [9–11] and cryptography [12], two-dimensional entanglement of high quanta of OAM [13,14], and entanglement of three-dimensional structures [15], as well as quantum communication in free space [16,17]. The $\mathrm{LG}_{n,\mathrm{l}}$ modes are described by two quantum numbers, n and l. They have $(n+1)$ intensity rings [18] and a central phase vortex with one singularity of order l [19]. Singularities, the centers of phase vortices, are points where the phase is undefined. Their order corresponds to the topological charge of the mode.

Here we focus on modes that can have very complex vortex and singularity patterns—the so-called Ince-Gauss (IG) modes [20,21], which are a natural generalization of LG modes in elliptic coordinates. In addition to the two quantum numbers of LG modes, they have one additional continuous parameter: the ellipticity ε [22]. Each value of the ellipticity defines a different complete orthonormal basis set; the LG modes emerge as a special case for $\varepsilon = 0$. The ellipticity leads to several unique phenomena, such as the splitting of the singularity of LG modes with topological charge l into l separate singularities each with unit topological charge, and the formation of additional singularities in the outer rings [23,24]. The number of singularities can be defined by choosing the topological charge and their positions can be adjusted by varying the ellipticity. Here we present the first quantum experiment with Ince-Gauss modes [25]. It is well known from the famous EPR (Einstein, Podolsky, and Rosen) gedankenexperiment [26] that a measurement of one particle immediately defines the state of its entangled partner. In our experiment such a measurement of a specific singularity pattern on one side defines the singularity structure of the distant photon, while such a singularity structure was not an element of reality before.

In the following we describe experiments in which we measure IG-qubit coincidence fringes and use a two-dimensional entanglement witness and a steering inequality to verify entanglement and nonlocal steering of complex singularity patterns. Then we record the coincidences for the same mode numbers, but with different ellipticities ε. This effect is unique for IG modes, and might be used in novel quantum information protocols. In the end, we introduce a new method to prove entanglement based on a three-dimensional entanglement witness, and therewith verify that the produced state is entangled in a higher-dimensional Hilbert space.

II. INCE-GAUSS MODES

Ince-Gauss modes are the natural solutions of the paraxial wave equation in elliptical coordinate systems. The two-dimensional elliptical coordinate system is described by the radial and angular elliptic coordinate u and v. In the waist plane $z = 0$ the transformation between elliptical (u, v) and Cartesian (x, y) coordinates is given by

$$\begin{pmatrix} x \\ y \end{pmatrix} = f_0 \begin{pmatrix} \cosh(u)\cos(v) \\ \sinh(u)\sin(v) \end{pmatrix}. \tag{1}$$

f_0 is the semifocal separation (eccentricity) of the coordinate system. A separation ansatz is used to solve the paraxial wave equation in elliptical coordinates [27,28]. This leads to the Ince equation which can be solved by the Ince polynomials,

*Corresponding authors: mario.krenn@univie.ac.at and anton.zeilinger@univie.ac.at

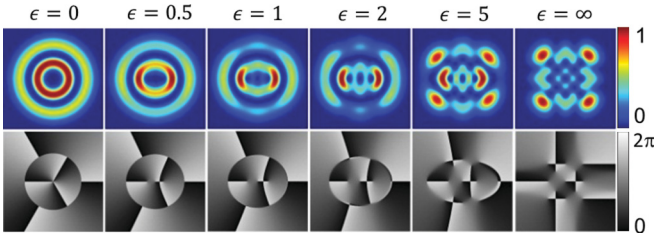

FIG. 1. (Color online) Ince-Gauss modes of varying ellipticity. The mode $\mathrm{IG}_{5,3,\varepsilon}$ has two rings and three central singularities. In the upper (lower) row the intensity (phase) distribution of each mode is shown. From left to right the values of ε are 0, 0.5, 1.0, 2.0, 5.0, ∞. The splitting of the phase singularity in the center into three singularities on a horizontal line can be observed as well as the creation of additional pairs of singularities in the ring of zero intensity [23]. For $\varepsilon = 0$, the IG beam becomes a Laguerre-Gauss mode with continuous rotational symmetry of the intensity pattern. For $\varepsilon > 0$, only a twofold rotational symmetry remains. In the limit of $\varepsilon \to \infty$, a fourfold rotational symmetry emerges; the corresponding modes are called helical Hermite-Gauss modes [30].

and gives the even and odd Ince-Gauss modes [20],

$$\mathrm{IG}^{e}_{p,m,\varepsilon}(\vec{r}) = N_e C^m_p(iu,\varepsilon) C^m_p(v,\varepsilon) \exp\left(-\frac{r^2}{\omega_0^2}\right), \qquad (2)$$

$$\mathrm{IG}^{o}_{p,m,\varepsilon}(\vec{r}) = N_o S^m_p(iu,\varepsilon) S^m_p(v,\varepsilon) \exp\left(-\frac{r^2}{\omega_0^2}\right). \qquad (3)$$

$\varepsilon = \frac{2f_0}{\omega_0^2}$ is the ellipticity parameter, ω_0 is the beam radius at the waist, and p and m are the IG mode indices with integer values. For equal ellipticity, modes with different p or m are orthogonal. As p and m both can take any positive integer value, they define an infinite-dimensional Hilbert space. The expressions $C^m_p(u,\varepsilon)$ and $S^m_p(u,\varepsilon)$ are the even and odd Ince polynomials; N_e and N_o are normalization constants. Then the helical Ince-Gauss (further referred to as Ince-Gauss) modes can be defined as superpositions of even and odd Ince-Gauss modes [29],

$$\mathrm{IG}^{\pm}_{p,m,\varepsilon}(\vec{r}) = \frac{1}{\sqrt{2}}\left(\mathrm{IG}^{e}_{p,m,\varepsilon}(\vec{r}) \pm i\,\mathrm{IG}^{o}_{p,m,\varepsilon}(\vec{r})\right). \qquad (4)$$

Taking the limit $\varepsilon \to 0$, Ince-Gauss modes become Laguerre-Gauss modes with an integer OAM value $l = m$, with the central singularities moving to the center of the beam. In the limit of $\varepsilon \to \infty$, the Ince-Gauss modes become "helical" Hermite-Gauss modes [30]. This transition can be seen in Fig. 1.

III. EXPERIMENTS

In our experimental setup (Fig. 2), we employ type-II spontaneous parametric down-conversion (SPDC) in a nonlinear crystal (periodically poled potassium titanyl phosphate, ppKTP) which creates pairs of photons. The two photons are collinear and have orthogonal polarizations. We split the photons with a polarizing beam splitter. In the two arms of the setup we analyze them by using a combination of spatial light modulators (SLMs) and single-mode fibers (SMFs). A SLM is a liquid crystal display, which can perform an arbitrary phase transformation on the incoming beam. In our experiment

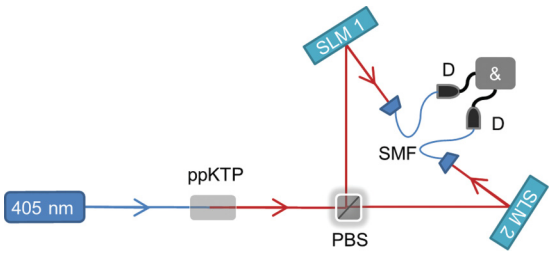

FIG. 2. (Color online) Schematic sketch of the experimental setup. We pump a 5-mm nonlinear ppKTP crystal with a 405-nm 60-mW single-mode diode laser, and obtain 810-nm down-converted spatially entangled photons of orthogonal polarization. We separate the two photons on a polarizing beam splitter (PBS), and manipulate their spatial mode using spatial light modulators (SLM), which transform specific Ince-Gauss modes into Gauss modes. The photons in the Gauss modes are then filtered by coupling into single-mode fibers (SMF). Finally, they are detected with avalanche photodiodes (D) and analyzed with a coincidence-logic (&) with around 5-ns coincidence window. The SLMs are in the far field of the crystal, and the SMFs are in the far field of the SLMs.

we use computer-generated holograms to convert specific higher-order modes into a Gauss mode, which we couple into a SMF. Since the SMFs only allow coupling of Gauss modes, we thereby realize a spatial-mode-specific filter. The photons are then detected with single-photon detectors and pairs are counted using a coincidence logic.

A. Two-dimensional entanglement

In the first experiment, we restrict ourselves to a two-dimensional Hilbert space, where we define a Bloch sphere analogously to the one representing the polarization of photons (Fig. 3). The poles are helical IG modes; each point on the equator represents a specific superposition with a well defined phase. The whole Bloch sphere can be represented by

$$\mathrm{IG}^{a,\phi}_{p,m,\varepsilon}(\vec{r}) = \left(\sqrt{a}\exp(i\phi)\mathrm{IG}^{+}_{p,m,\varepsilon}(\vec{r}) + \sqrt{1-a}\exp(-i\phi)\mathrm{IG}^{-}_{p,m,\varepsilon}(\vec{r})\right), \qquad (5)$$

where a goes from 0 to 1, and φ goes from 0 to π.

As a specific example, we analyze the $\mathrm{IG}^{a,\varphi}_{5,32}$ mode, which has two rings and three split singularities with an ellipticity $\varepsilon = 2$ [Fig. 3(a)]. On both SLMs we display the phase pattern for states at the equator of the Bloch sphere. The hologram for four specific phases φ is displayed at the SLM1, while the SLM2 scans through the holograms for phases from $\varphi = 0$ to $\varphi = 180°$. In Figs. 3(b) and 4 the coincidence counts are shown as a function of the phase of the hologram displayed at SLM2. We observe nonclassical two-photon fringes, with a high visibility.

For quantifying the entanglement, we take advantage of an entanglement witness operator [31]. Similar to entangled OAM states from down-conversion, we expect a Bell state close to $|\psi_+\rangle$ of the down-converted photon pair. Therefore a suitable witness operator for detecting entanglement in this state can be written as

$$\hat{W} = \tfrac{1}{4}(1 - \sigma_x \otimes \sigma_x - \sigma_y \otimes \sigma_y + \sigma_z \otimes \sigma_z), \qquad (6)$$

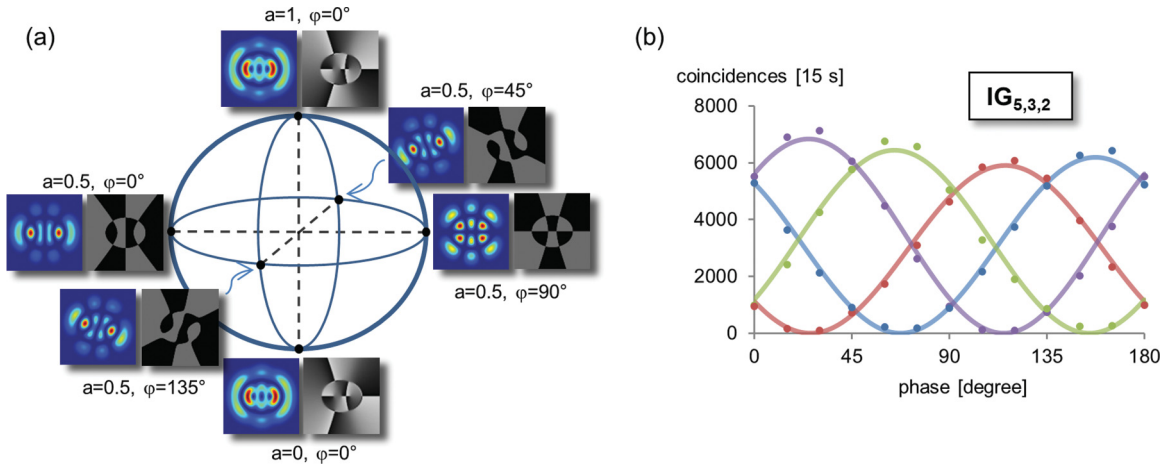

FIG. 3. (Color online) (a) Bloch sphere constructed from the Ince-Gauss modes $IG_{5,3,2}$ with two rings and three phase singularities. The insets show the intensity (left) and phase patterns (right). Similarly to the Laguerre-Gauss (LG) modes, the intensity patterns at the north and south poles are identical. However, in contrast to LG modes, where a continuous phase change of φ along the equator only leads to a rotation of the phase and intensity pattern, these patterns also change their shape continuously. The consequence is a different decomposition into LG modes, which leads to additional effects for nonmaximal entangled LG states such as those from down-conversion. (b) Coincidence fringes for the $IG_{5,3,2}$ mode with four different settings for the signal photon (22.5°, 67.5°, 112.5°, and 157.5°, respectively) and 15° phase steps of the superposition for the idler, with $\sin^2$ fits. Each point has been measured for 15 s. We estimate the statistical uncertainty assuming a Poisson distribution of the count rates and obtained error bars are smaller than the symbols in the figure.

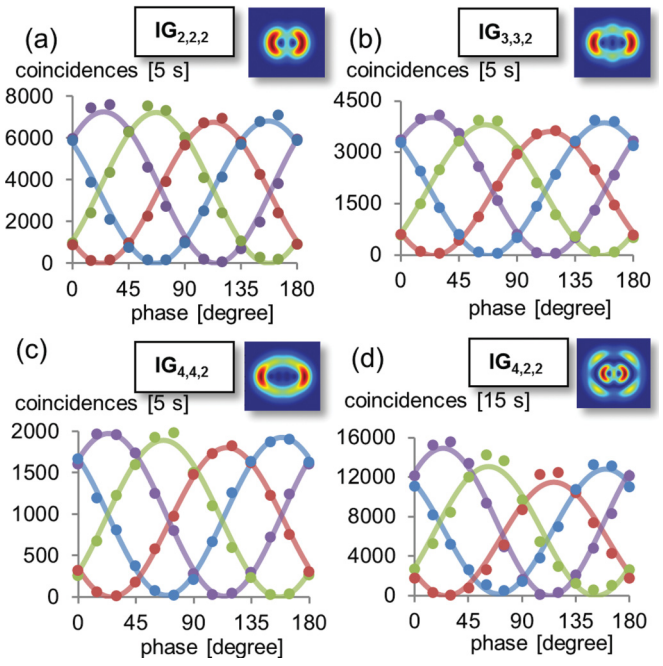

FIG. 4. (Color online) Coincidence fringes for different Ince-Gauss modes with ellipticity $\varepsilon = 2$. Panels (a), (b), and (c) have two, three, and four singularities, respectively, and no additional rings, and each data point has been measured for 5 s. Panel (d) has two singularities and one additional ring. Each point has been measured for 15 s. The different fringes correspond to the measurement setting of the SLM2 (22.5°, 67.5°, 112.5°, and 157.5°, respectively). The obtained error bars from Poisson distribution are smaller than the symbols in the figure. The lines show sinusoidal fits. We expect the different sinusoidal amplitudes as well as the deviation of the experimental points from the sinusoidal fits to be due to the plane-wave approximation used in programming the holograms.

where σ_x, σ_y, and σ_z denote the single-qubit Pauli matrices for the two photons. The witness operator is defined to be positive for all separable states, and will give $\langle W \rangle = -0.5$ for the maximally entangled state. Recently it was shown that there exist systems that are entangled while the state of the distant photon cannot be steered [32]. We show the violation of a steering inequality to verify that by measuring one photon, we can nonlocally steer the singularity structure of its entangled partner. For that we use an inequality that has been derived recently [33,34], namely $S = |\sigma_x \otimes \sigma_x|^2 + |\sigma_y \otimes \sigma_y|^2 + |\sigma_z \otimes \sigma_z|^2 < 1$ that holds for all nonsteerable states. The values of the entanglement witness W and the steering value S calculated from our measurement results are given in Table I. The witness $\langle W \rangle$ for every measured mode is negative, which verifies entanglement for the generated states. Furthermore the steering value S is bigger than 1, which

TABLE I. Entanglement witness and steering value for five different Ince-Gauss modes. For five different IG modes we have measured the entanglement witness as described in Eq. (6). The negative witness value verifies entanglement of our state. The steering value S is above the nonsteerable limit of $S < 1$, which verifies that by measuring one photon we can nonlocally steer the singularity pattern of the second photon. The statistical uncertainty given in parentheses has been calculated assuming Poisson distributed statistics.

IG parameters	Witness $\langle W \rangle$	Steering value S
$p = 2, m = 2, \varepsilon = 2$	$-0.4847(3)$	2.879(2)
$p = 3, m = 3, \varepsilon = 2$	$-0.4897(3)$	2.918(2)
$p = 4, m = 4, \varepsilon = 2$	$-0.4905(4)$	2.925(3)
$p = 4, m = 2, \varepsilon = 2$	$-0.4581(7)$	2.675(5)
$p = 5, m = 3, \varepsilon = 2$	$-0.4784(7)$	2.830(5)

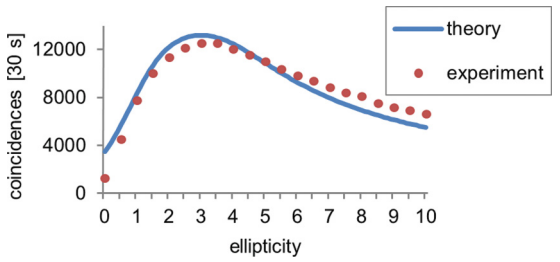

FIG. 5. (Color online) Overlap between two Ince-Gauss modes with the same value of p and m, but different ellipticities. This measurement shows a unique behavior of Ince-Gauss modes, which might be useful for quantum communication applications. The horizontal axis is the ellipticity; the vertical axis shows the coincidence counts. The blue line shows the theoretical overlap $|\langle \mathrm{IG}_{8,4,3}|\mathrm{IG}_{8,4,\varepsilon}\rangle|^2$, where the maximal overlap is at $\varepsilon = 3$. The red dots are measured coincidence counts, which show good agreement to the theoretical values. The obtained error bars are smaller than the symbols in the figure.

demonstrates that we are able to nonlocally steer the singularity pattern of the distant photon.

B. Specific quantum-correlation function

In our second experiment we analyze the correlation between two down-converted photons when projected onto Ince-Gauss modes with the same mode numbers, but with different ellipticity. The ellipticity is a unique feature of IG modes, which does not exist for LG modes. It can be understood as a continuous nontrivial rotation parameter for the infinite-dimensional basis of the Hilbert space. Thus by analyzing two modes with different ellipticities, we measure the overlap between continuously rotated basis elements.

As the basis rotation performed by the ellipticity parameter affects the whole infinite-dimensional Hilbert space, this has an interesting effect on two-dimensional subspaces. In contrast to simple two-dimensional systems such as polarization, a mode with a specific ellipticity cannot fully be reconstructed in the corresponding two-dimensional subspace with a different ellipticity. The projection into this basis gives a result smaller than 1, and therefore the coincidences are reduced. It might be possible to use this effect for extensions to quantum cryptography protocols such as BB84 or Ekert91 [35,36], for instance by a two-step protocol where in the first step the secret ellipticity is transmitted and in the second step the IG basis is used, and the second step uses IG modes with the ellipticity from step 1. An eavesdropper faces the additional task of getting the correct value of the ellipticity, and might gain less information for a wrong value. A full security proof is out of the scope of this work.

In the experiment, we display on SLM1 the phase pattern of an IG mode with a specific ellipticity, and on SLM2 we display the phase pattern of a mode with the same characteristic numbers p and m but different ε. When the two ε match, we measure a maximum coincidence count rate, whereas for different ellipticities ε and ε' the coincidence rate decreases. The decrease of the coincidence rate is bigger for higher modes; therefore we used $\mathrm{IG}_{8,4,\varepsilon}$. The calculated overlap, where we assume a maximally entangled state, and the measured coincidence counts are shown in Fig. 5.

The overlap between two Ince-Gauss modes with different ellipticities has been calculated in Fig. 6 for three different quantum numbers. It can be observed that the overlap drops faster for higher-order modes. This can be understood when taking into account that the expansion into the Laguerre-Gauss basis involves more terms the higher the Ince-Gauss modes are. For example, for IG $p = 14$, $m = 6$, the overlap drops very fast and reaches zero for a finite ellipticity, before it increases again. The vanishing overlap indicates orthogonal modes with the same quantum numbers (same number of initial rings and singularities). It might be interesting to investigate whether one can find multiple orthogonal modes and whether there are nontrivial relations between those orthogonal modes.

C. Higher-dimensional entanglement

Finally, in our third experiment, we verify that the photons are indeed entangled in a higher-dimensional Hilbert space. For this task, we use the first nontrivial three-dimensional

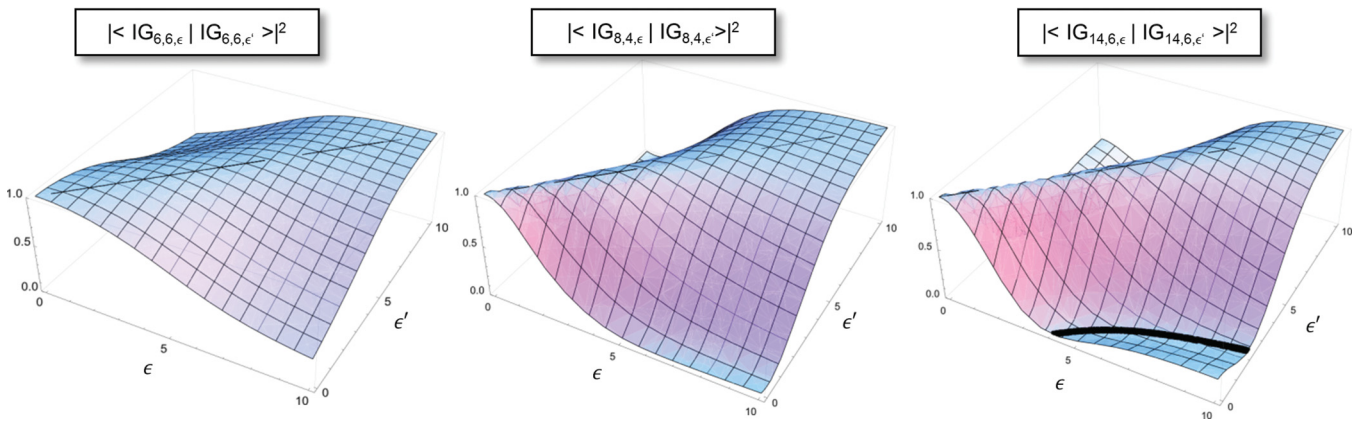

FIG. 6. (Color online) Overlap between Ince-Gauss modes with the same quantum numbers but different ellipticity. When the ellipticities match, the overlap is maximal. When the ellipticities are different, the overlap decreases. The higher the quantum number, the faster the overlap decreases. For $p = 14$, $m = 6$, the overlap reaches zero (black line) and then increases again. This vanishing overlap indicates orthogonal modes (with the same quantum number).

Ince-Gauss space. A state in such a space can be written as

$$|\psi\rangle = a|\mathrm{IG}^{+}_{2,2,5},\mathrm{IG}^{-}_{2,2,5}\rangle + b|\mathrm{IG}^{+}_{3,3,5},\mathrm{IG}^{-}_{3,3,5}\rangle + c|\mathrm{IG}^{+}_{4,4,5},\mathrm{IG}^{-}_{4,4,5}\rangle, \quad (7)$$

where a, b, and c are probabilities for specific modes, due to the spiral bandwidth of the SPDC process [37–39]. Similarly to the two-dimensional case, we can define an entanglement witness for three dimensions, which consists of the visibilities in three mutually unbiased bases for every two-dimensional subspace [40,41]. The simplest correlation function of this type can be written as

$$f(\rho) = \sum_{l=3}^{4}\sum_{k=2}^{k<l}\frac{1}{N_{k,l}}\left(\left\langle\sigma_{x}^{k,l}\otimes\sigma_{-x}^{k,l}\right\rangle + \left\langle\sigma_{y}^{k,l}\otimes\sigma_{-y}^{k,l}\right\rangle + \left\langle\sigma_{z}^{k,l}\otimes\sigma_{-z}^{k,l}\right\rangle\right). \quad (8)$$

The $\sigma_{\pm i}$ is a Pauli matrix constructed from $\mathrm{IG}^{\pm}$ and denotes the measurements in the mutually unbiased bases of a two-dimensional subspace of the three-dimensional state. $N_{k,l}$ are normalization constants that appear because we ignore the third degree of freedom in the two-dimensional measurement.

Due to the unavoidable normalization of the two-dimensional subspaces, bounding this correlation function for separable and two-dimensionally entangled states becomes a challenging task. The function itself is neither linear nor convex, inevitably excluding all previously known techniques to bound such functions. We were able to prove analytical bounds for the correlation function (for details and the full analytical proof see Supplemental Material [42]). The results are

Limit for separable states: $f(\rho) = 3$.

Limit for two-dimensionally entangled states: $f(\rho) = 6$.

Overall maximum: $f(\rho) = 9$.

Inserting the measured visibilities into the correlation function in Eq. (8) gives the value $f(\rho) = 8.156(5)$ which is well above the limit $f(\rho) = 6$ for an entangled state in two dimensions, and therefore shows that the measured state was at least a three-dimensionally entangled state. In addition, one can use the ellipticity to tune the detection probability of higher-order spatial modes (see Fig. 7), for instance, to experimentally access higher-order modes than with LG modes. This might be useful for down-conversion experiments that deal with high mode numbers such as high-dimensional entanglement detection, due to the potential increase of detected count rates.

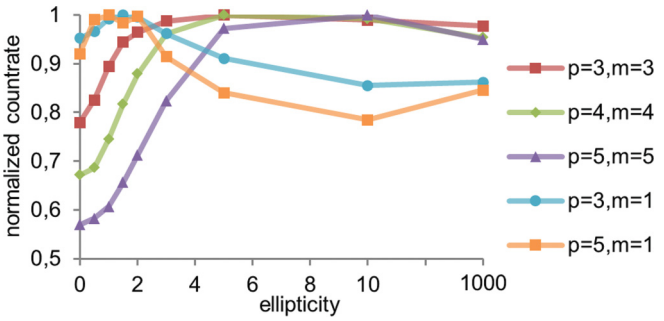

FIG. 7. (Color online) Normalized coincidence count rates of several different Ince-Gauss modes depending on the ellipticity. For five different fixed p and m quantum number combination and nine values of the ellipticity, coincidence counts have been measured. For every quantum number combination, the coincidence counts have been normalized to the maximum value of the nine measurements with different ellipticity. It is shown that the probability of modes from the down-conversion can be tuned by adjusting the ellipticity of the basis. The effect is stronger for higher modes, which is crucial for high-dimensional entanglement detection. The obtained error bars are in the range of 1%, and therefore smaller than the symbols in the figure.

IV. CONCLUSIONS

We have shown the entanglement of photons with adjustable singularity and vortex structures. By measuring a singularity pattern for the first photon we nonlocally steer the positions of multiple singularities on the second photon. Additionally, we measured an IG-specific coincidence function depending on the ellipticity, which could be used for quantum information tasks. We also introduced a method for detecting three-dimensional entanglement, and verified therewith three-dimensional entanglement.

We suggest that the detection probability of higher-order modes from SPDC can be tuned with the ellipticity parameter, which might be useful for experiments that deal with high-order modes. Furthermore, due to the nontrivial basis rotation of the Hilbert space, we believe that this additional parameter could be used to extend well-known quantum key distribution protocols.

ACKNOWLEDGMENTS

This work was supported by the ERC Advanced Grant No. QIT4QAD, and the Austrian Science Fund FWF within the SFB F40 (FoQuS) and W1210-2 (CoQuS). M.H. gratefully acknowledges support from the EC project "IP Q-Essence" and the ERC (Advanced Grant "IRQUAT"). We acknowledge C. Schaeff for discussion of the high-dimensional entanglement.

[1] *The Physics of Quantum Information*, edited by D. Bouwmeester, A. Ekert, and A. Zeilinger (Springer, Berlin, 2000).

[2] S. J. Freedman and J. F. Clauser, Phys. Rev. Lett. **28**, 938 (1972).

[3] P. G. Kwiat, A. M. Steinberg, and R. Y. Chiao, Phys. Rev. A **47**, R2472 (1993).

[4] J. G. Rarity and P. R. Tapster, Phys. Rev. Lett. **64**, 2495 (1990).

[5] S. Ramelow, L. Ratschbacher, A. Fedrizzi, N. K. Langford, and A. Zeilinger, Phys. Rev. Lett. **103**, 253601 (2009).

[6] A. Mair, A. Vaziri, G. Weihs, and A. Zeilinger, Nature **412**, 313 (2001).

[7] G. Molina-Terriza, J. P. Torres, and L. Torner, Nat. Phys. **3**, 305 (2007).
[8] A. M. Yao and M. J. Padgett, Adv. Opt. Photonics **3**, 161 (2011).
[9] A. Vaziri, G. Weihs, and A. Zeilinger, Phys. Rev. Lett. **89**, 240401 (2002).
[10] B.-J. Pors, F. Miatto, G. W. 't Hooft, E. R. Eliel, and J. P. Woerdman, J. Opt. **13**, 064008 (2011).
[11] A. C. Dada, J. Leach, G. S. Buller, M. J. Padgett, and E. Andersson, Nat. Phys. **7**, 677 (2011).
[12] S. Gröblacher, T. Jennewein, A. Vaziri, G. Weihs, and A. Zeilinger, New J. Phys. **8**, 75 (2006).
[13] J. Leach, B. Jack, J. Romero, M. Ritsch-Marte, R. W. Boyd, A. K. Jha, S. M. Barnett, S. Franke-Arnold, and M. J. Padgett, Opt. Express **17**, 8287 (2009).
[14] R. Fickler, R. Lapkiewicz, W. N. Plick, M. Krenn, C. Schaeff, S. Ramelow, and A. Zeilinger, Science **338**, 640 (2012).
[15] J. Romero, J. Leach, B. Jack, M. R. Dennis, S. Franke-Arnold, S. M. Barnett, and M. J. Padgett, Phys. Rev. Lett. **106**, 100407 (2011).
[16] B.-J. Pors, C. H. Monken, E. R. Eliel, and J. P. Woerdman, Opt. Express **19**, 6671 (2011).
[17] M. Malik, M. O'Sullivan, B. Rodenburg, M. Mirhosseini, J. Leach, M. P. J. Lavery, M. J. Padgett, and R.W. Boyd, Opt. Express **20**, 13195 (2012).
[18] V. D. Salakhutdinov, E. R. Eliel, and W. Löffler, Phys. Rev. Lett. **108**, 173604 (2012).
[19] L. Allen, M. W. Beijersbergen, R. J. C. Spreeuw, and J. P. Woerdman, Phys. Rev. A **45**, 8185 (1992).
[20] M. A. Bandres and J. C. Gutiérrez-Vega, Opt. Lett. **29**, 144 (2004).
[21] M. A. Bandres and J. C. Gutiérrez-Vega, J. Opt. Soc. Am. A **21**, 873 (2004).
[22] M. A. Bandres and J. C. Gutiérrez-Vega, Opt. Express **16**, 21087 (2008).
[23] S. Lopez-Aguayo and J. C. Gutiérrez-Vega, Opt. Express **15**, 18326 (2007).
[24] W. N. Plick, M. Krenn, R. Fickler, S. Ramelow, and A. Zeilinger, arXiv:1208.1865.
[25] M. Krenn, R. Fickler, W. Plick, R. Lapkiewicz, S. Ramelow, and A. Zeilinger, Bull. Am. Phys. Soc. **57**, Abstract W1.00006 (2012).
[26] A. Einstein, B. Podolsky, and N. Rosen, Phys. Rev. **47**, 777 (1935).
[27] E. Ince, Proc. London Math. Soc. **23**, 56 (1923).
[28] F. Arscott, *Periodic Differential Equations* (Pergamon Press, New York, 1964).
[29] J. B. Bentley, J. A. Davis, M. A. Bandres, and J. C. Gutiérrez-Vega, Opt. Lett. **31**, 649 (2006).
[30] C. López-Mariscal and J. C. Gutiérrez-Vega, Proc. SPIE **6663**, 666307-1 (2007).
[31] O. Gühne and G. Tóth, Phys. Rep. **474**, 1 (2009).
[32] D. J. Saunders, S. J. Jones, H. M. Wiseman, and G. J. Pryde, Nat. Phys. **6**, 845 (2010).
[33] D. H. Smith, G. G. Gillett, M. P. Almeida, C. Branciard, A. Fedrizzi, T. J. Weinhold, A. Lita, B. Calkins, T. Gerrits, S-W. Nam, and A. G. White, Nat. Commun. **3**, 625 (2012).
[34] B. Wittmann, S. Ramelow, F. Steinlechner, N. K. Langford, N. Brunner, H. Wiseman, R. Ursin, and A. Zeilinger, New J. Phys. **14**, 053030 (2012).
[35] C. H. Bennett and G. Brassard, in *Proceedings of the IEEE International Conference on Computers, Systems, and Signal Processing, Bangalore, India*, 1984, p. 175.
[36] A. K. Ekert, Phys. Rev. Lett. **67**, 661 (1991).
[37] F. M. Miatto, A. M. Yao, and S. M. Barnett, Phys. Rev. A **83**, 033816 (2011).
[38] H. Di Lorenzo Pires, H. C. B. Florijn, and M. P. van Exter, Phys. Rev. Lett. **104**, 020505 (2010).
[39] E. Brambilla, L. Caspani, L. A. Lugiato, and A. Gatti, Phys. Rev. A **82**, 013835 (2010).
[40] C. Spengler, M. Huber, A. Gabriel, and B. Hiesmayr, Quantum Inf. Process. doi: 10.1007/s11128-012-0369-8 (2012).
[41] J. I. de Vicente and M. Huber, Phys. Rev. A **84**, 062306 (2011).
[42] See Supplemental Material at http://link.aps.org/supplemental/10.1103/PhysRevA.87.012326 for full analytical proof of the bounds of the correlation function.